



## High-temperature Thermoelectric and Microstructural Characteristics of Ga Substituted on the Co-site in Cobalt-based Oxides

Van Nong, Ngo; Yanagiya, S.; Sonne, Monica; Pryds, Nini; Ohtaki, M.

*Published in:*  
Journal of Electronic Materials

*Link to article, DOI:*  
[10.1007/s11664-011-1524-1](https://doi.org/10.1007/s11664-011-1524-1)

*Publication date:*  
2011

[Link back to DTU Orbit](#)

*Citation (APA):*  
Van Nong, N., Yanagiya, S., Sonne, M., Pryds, N., & Ohtaki, M. (2011). High-temperature Thermoelectric and Microstructural Characteristics of Ga Substituted on the Co-site in Cobalt-based Oxides. *Journal of Electronic Materials*, 40(5), 716-722. <https://doi.org/10.1007/s11664-011-1524-1>

---

### General rights

Copyright and moral rights for the publications made accessible in the public portal are retained by the authors and/or other copyright owners and it is a condition of accessing publications that users recognise and abide by the legal requirements associated with these rights.

- Users may download and print one copy of any publication from the public portal for the purpose of private study or research.
- You may not further distribute the material or use it for any profit-making activity or commercial gain
- You may freely distribute the URL identifying the publication in the public portal

If you believe that this document breaches copyright please contact us providing details, and we will remove access to the work immediately and investigate your claim.

# High-Temperature Thermoelectric and Microstructural Characteristics of Cobalt-Based Oxides with Ga Substituted on the Co-Site

N.V. NONG,<sup>1,4</sup> S. YANAGIYA,<sup>1,2</sup> S. MONICA,<sup>1</sup> N. PRYDS,<sup>1</sup> and M. OHTAKI<sup>3</sup>

1.—Division of Fuel Cells and Solid State Chemistry, Risø National Laboratory for Sustainable Energy, Technical University of Denmark, 4000 Roskilde, Denmark. 2.—Department of Electrical and Electronic Engineering, Hakodate National College of Technology, 14-1 Tokura, Hakodate, Hokkaido 042-8501, Japan. 3.—Interdisciplinary Graduate School of Engineering Sciences, Kyushu University, Fukuoka 816-8580, Japan. 4.—e-mail: nngo@risoe.dtu.dk

The effects of Ga substitution on the Co-site on the high-temperature thermoelectric properties and microstructure are investigated for the misfit-layered  $\text{Ca}_3\text{Co}_4\text{O}_9$  and the complex perovskite-related  $\text{Sr}_3\text{RECo}_4\text{O}_{10.5}$  (RE = rare earth) cobalt-based oxides. For both systems, substitution of Ga for Co results in a simultaneous increase in the Seebeck coefficient ( $S$ ) and the electrical conductivity ( $\sigma$ ), and the influence is more significant in the high temperature region. The power factor ( $S^2\sigma$ ) is thereby remarkably improved by Ga substitution, particularly at high temperatures. Texture factor calculations using x-ray diffraction pattern data for pressed and powder samples reveal that the Ga-doped samples are highly textured. Microstructure observed by scanning electron microscopy shows very well-crystallized grains for the samples with Ga substitution for Co. Among the Ga-doped samples,  $\text{Ca}_3\text{Co}_{3.95}\text{Ga}_{0.05}\text{O}_9$  shows the best  $ZT$  value of 0.45 at 1200 K, which is about 87.5% higher than the nondoped one, a considerable improvement.

**Key words:** Cobalt oxides, hot pressing, electrical conductivity, figure of merit

## INTRODUCTION

Cobalt oxides form a large family of compounds with fascinating structural and physical properties. The different possible oxidation states of cobalt (divalent, trivalent, and tetravalent) together with its various spin configurations (for example, low spin, intermediate spin, and high spin) for Co ions are responsible for various interesting phenomena such as temperature-induced spin-state transitions in oxides with perovskite-like structure such as  $\text{LaCoO}_3$ <sup>1</sup> and  $\text{Sr}_{1-x}\text{Y}_x\text{CoO}_{3-\delta}$ ,<sup>2</sup> giant magnetoresistance in  $\text{La}_{1-x}\text{Sr}_x\text{CoO}_3$ ,<sup>3</sup> and unusual thermoelectric properties (coexistence of large thermoelectric power and low electrical resistivity) in the misfit-layered cobalt oxides<sup>4,5</sup>  $\text{NaCo}_2\text{O}_4$  and  $\text{Ca}_3\text{Co}_4\text{O}_9$ . Many attempts have been made to optimize the

thermoelectric performance of these compounds by either ion doping or improving fabrication methods. While most investigations have mainly concentrated on the effects of substitution on the A-site in perovskite-related systems<sup>6-8</sup> or Ca-site in misfit-layered systems,<sup>9-13</sup> a few groups have performed substitution on the Co-site.<sup>14-16</sup> The peculiar structural arrangement of the  $\text{CoO}_6$  octahedra, containing cobalt cations with mixed valence of 3+ and 4+, is the origin of the interesting properties of those cobaltites. Ion doping on the Co-sites, especially Co ion in the  $\text{CoO}_6$  octahedra isostructural to the  $\text{CoO}_2$  planes, possibly induces more notable effects on the transport and thermoelectric properties of these materials as the charge-carrier transport mostly occurs within these layers. Previous reports have shown that substitutions at Co-site by Zr in  $(\text{La,Sr})\text{CoO}_3$ <sup>14</sup> and by Fe in misfit-layered  $\text{Ca}_3\text{Co}_4\text{O}_9$ <sup>15</sup> are effective in improving the thermoelectric properties of these materials.

(Received May 11, 2010; accepted January 17, 2011)



67 In this work, the Co-site of the complex perovskite-related  $\text{Sr}_3\text{RECo}_4\text{O}_{10.5}$  (RE = Y and Gd) and  
68 the misfit-layered  $\text{Ca}_3\text{Co}_4\text{O}_9$  cobalt oxides was  
69 substituted with Ga. The effects of Ga doping on the  
70 microstructure and the high-temperature thermo-  
71 electric properties of these systems are systemati-  
72 cally investigated and discussed.  
73

## 74 EXPERIMENTAL PROCEDURES

75 Polycrystalline samples of  $\text{Ca}_3\text{Co}_{4-x}\text{Ga}_x\text{O}_9$  ( $0 \leq$   
76  $x \leq 0.2$ ) and  $\text{Sr}_3\text{RECo}_{4-x}\text{Ga}_x\text{O}_{10.5}$  with RE = Y and  
77 Gd ( $0 \leq x \leq 0.3$ ) were synthesized by solid-state  
78 reaction from  $\text{CaCO}_3$ ,  $\text{SrCO}_3$ ,  $\text{RE}_2\text{O}_3$ ,  $\text{Co}_3\text{O}_4$ , and  
79  $\text{Ga}_2\text{O}_3$ . Synthesized powders of  $\text{Sr}_3\text{RECo}_{4-x}\text{Ga}_x\text{O}_{10.5}$   
80 were pressed into pellets under cold isostatic pres-  
81 sure of 250 MPa followed by a sintering process at  
82 1423 K for 24 h after the mixed powders were  
83 calcined at 1373 K for 24 h in air. As for the  
84  $\text{Ca}_3\text{Co}_{4-x}\text{Ga}_x\text{O}_9$  system, the samples after sintering  
85 at 1173 K for 48 h with intermediate grinding were  
86 reground then hot-pressed into pellets at 1123 K  
87 under uniaxial pressure of 60 MPa for 2 h in air.  
88 The phase purity was checked by powder x-ray dif-  
89 fraction (XRD) measurements using a Bruker D8  
90 diffractometer with Cu K $\alpha$  radiation. Structure  
91 refinements were analyzed using *Jana2006* crys-  
92 tallographic software for the powder XRD data.  
93 Density of the samples was determined using the  
94 Archimedes method. The microstructure of the  
95 samples was observed by using a Hitachi scanning  
96 electron microscopy (TM-1000) system. The electri-  
97 cal resistivity and thermoelectric power were mea-  
98 sured simultaneously from room temperature to  
99 1200 K using an ULVAC-RIKO ZEM3 thermoelec-  
100 tric property measurement system in a low-pressure  
101 helium atmosphere. The thermal conductivity was  
102 determined from the thermal diffusivity and the  
103 specific heat capacity measured from room temper-  
104 ature to 1073 K using LFA-457 laser flash and DSC-  
105 404C thermal analysis measurement systems. The  
106 carrier concentrations and mobility of samples were  
107 measured at room temperature by Hall measure-  
108 ments with applied field of 0.55 T using the van der  
109 Pauw method.

## 110 RESULTS AND DISCUSSION

111 XRD analysis at room temperature revealed that  
112 nondoped and Ga-doped samples of the  $\text{Sr}_3\text{RE-}$   
113  $\text{Co}_{4-x}\text{Ga}_x\text{O}_{10.5}$  system are single phase for  $x \leq 0.1$ .  
114 However, a small impurity peak could be observed  
115 for samples with higher Ga content, e.g., for  $x = 0.2$   
116 and 0.3 samples, and the intensity of this peak in-  
117 creased with increasing Ga concentration. As for the  
118  $\text{Ca}_3\text{Co}_{4-x}\text{Ga}_x\text{O}_9$  system, the structure refinement  
119 was analyzed by using *Jana2006* Rietveld software  
120 with input parameters taken from Grebille et al.<sup>17</sup>  
121 using the superspace group  $X2/m(0, \delta, 0)s0$ , which is  
122 the standard setting of the superspace group  $C2/$   
123  $m(1, \delta, 0)s0$ . The calculated and the difference pro-  
124 files ( $R_p = 0.0573$ ,  $R_{wp} = 0.0793$ ) were found to be in

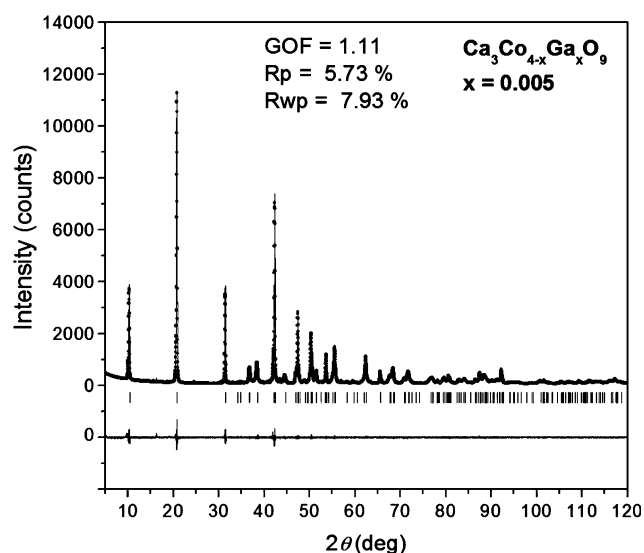


Fig. 1. Observed (dotted line), calculated (solid line), and difference powder XRD profiles ( $\lambda = 1.9604$  Å) for the final Rietveld refinement of a typical polycrystalline sample for  $\text{Ca}_3\text{Co}_{4-x}\text{Ga}_x\text{O}_9$  with  $x = 0.05$ .

good agreement with previous report,<sup>18</sup> confirming  
the  $\text{Ca}_3\text{Co}_{4-x}\text{Ga}_x\text{O}_{9+\delta}$  standard phase. Oxygen con-  
tent ( $9 + \delta$ ) was determined through iodometric  
titration, the  $\delta$  value being about 0.3 and the dif-  
ference between samples being less than 1%.  
Figure 1 shows the result for a typical Ga-doped  
sample with  $x = 0.05$ . The lattice constants for the  
 $x = 0$  sample were  $a = 4.8347(7)$  Å,  $b_1 = 4.5476(9)$  Å,  
 $b_2 = 2.819(1)$  Å,  $c = 10.8514(1)$  Å, and  $\beta = 98.12(6)^\circ$ .  
The lattice constants determined for the  $x = 0.05$   
sample were  $a = 4.8230(7)$  Å,  $b_1 = 4.5467(6)$  Å,  $b_2 =$   
 $2.807(1)$  Å,  $c = 10.8125(3)$  Å, and  $\beta = 98.06(2)^\circ$ . The  
structural parameters such as the misfit ratio  $b_1/b_2$ ,  
 $c$ , and  $\beta$  as indicated by these results are slightly  
distorted by the Ga doping.

Density of all the samples was measured using  
the Archimedes method, and the relative densities  
are listed in Table I. Under the same conditions of  
pressing and sintering processes, the  $\text{Sr}_3\text{RECo}_4\text{O}_{10.5}$   
sample with RE = Y exhibited a rather low relative  
density (65.6%) in comparison with the RE = Gd  
sample (88.8%). Notably, Ga doping results in a  
significant increase of the relative density, and the  
values tend to increase with increasing Ga concen-  
tration for the complex perovskite system. As for the  
layered cobaltite system, the densities of all nond-  
oped and Ga-doped samples were greater than 95%,  
and their difference was about  $\leq 1.2\%$ . The  $\text{Ca}_3$ -  
 $\text{Co}_{4-x}\text{Ga}_x\text{O}_9$  sample with  $x = 0.05$  had the highest  
relative density value of 96.5%.

Figure 2a–d shows scanning electron microscopy  
(SEM) images from fractured surfaces for  $\text{Sr}_3\text{Y-}$   
 $\text{Co}_4\text{O}_{10.5}$ ,  $\text{Sr}_3\text{YCo}_{3.9}\text{Ga}_{0.1}\text{O}_{10.5}$ ,  $\text{Sr}_3\text{GdCo}_4\text{O}_{10.5}$ , and  
 $\text{Sr}_3\text{GdCo}_{3.9}\text{Ga}_{0.1}\text{O}_{10.5}$  samples, respectively. Large  
pores can be clearly observed in the SEM image  
of  $\text{Sr}_3\text{YCo}_4\text{O}_{10.5}$  (Fig. 2a), while the size of the pores  
is much smaller for the  $\text{Sr}_3\text{GdCo}_4\text{O}_{10.5}$  sample



**Table I. Relative densities and thermoelectric (TE) characteristics of nondoped and Ga-doped samples**

Compositions	Relative Density (%)	$\sigma_{300K}$ (S/cm)	$S_{300K}$ ( $\mu V/K$ )	$\sigma_{1200K}$ (S/cm)	$S_{1200K}$ ( $\mu V/K$ )
$Sr_3YCo_4O_{10.5}$	65.6	3.6	67.1	126.6	14.3
$Sr_3YCo_{3.9}Ga_{0.1}O_{10.5}$	86.8	24.5	51.9	146.6	17.8
$Sr_3YCo_{3.8}Ga_{0.2}O_{10.5}$	87.3	18.1	23.0	125.4	23.7
$Sr_3YCo_{3.7}Ga_{0.3}O_{10.5}$	88.7	12.6	40.5	113.7	27.1
$Sr_3GdCo_4O_{10.5}$	88.3	3.0	72.7	372.5	14.1
$Sr_3GdCo_{3.9}Ga_{0.1}O_{10.5}$	90.0	11.9	146.8	379.7	32.7
$Ca_3Co_4O_9$	95.3	90.8	136.0	111.0	174.0
$Ca_3Co_{3.95}Ga_{0.05}O_9$	96.5	100.1	140.6	133.6	206.3
$Ca_3Co_{3.9}Ga_{0.1}O_9$	96.0	99.1	140.0	133.0	198.0
$Ca_3Co_{3.8}Ga_{0.2}O_9$	95.8	95.2	155.0	131.0	180.0

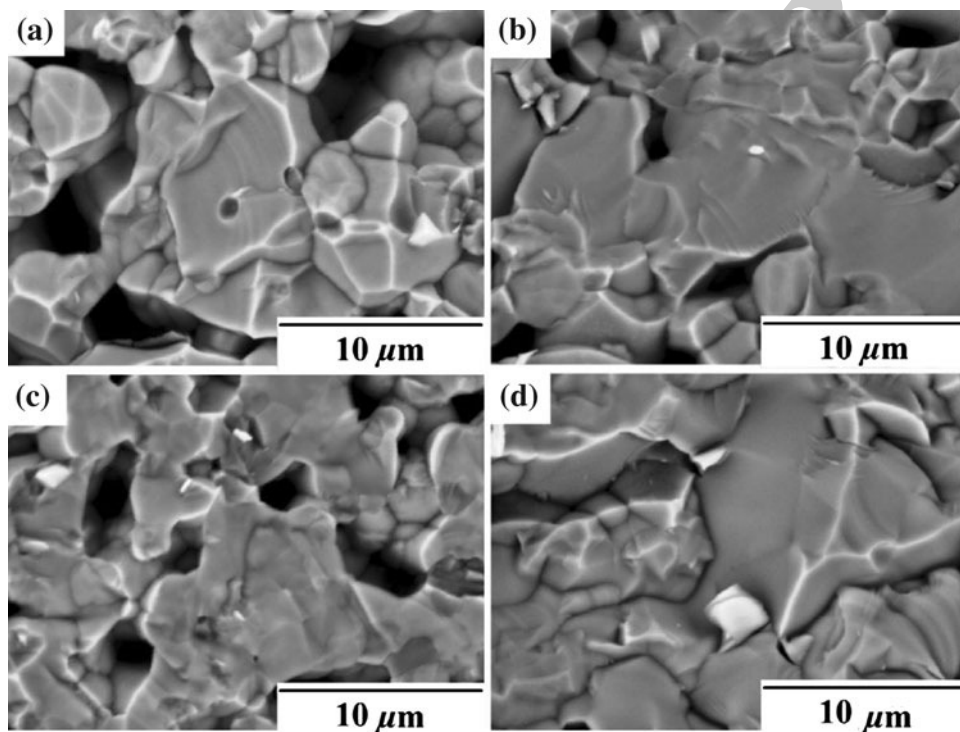


Fig. 2. SEM images from fractured surfaces of the samples for: (a)  $Sr_3YCo_4O_{10.5}$ , (b)  $Sr_3YCo_{3.9}Ga_{0.1}O_{10.5}$ , (c)  $Sr_3GdCo_4O_{10.5}$ , and (d)  $Sr_3GdCo_{3.9}Ga_{0.1}O_{10.5}$ .

162 (Fig. 2c). It is also very clear from Fig. 2b, d that the  
 163 SEM images of the Ga-doped samples show crys-  
 164 talline grains with well-developed crystal faces.  
 165 This result provides evidence for the difference of  
 166 relative densities among the samples, as afore-  
 167 mentioned. It also suggests that the samples with  
 168 Ga substitution are highly textured. To elucidate  
 169 the crystallographic texture, XRD analysis was  
 170 carried out on a pressed-surface pellet and on free  
 171 powder. A textured coefficient (TC) for each  $(hkl)_i$   
 172 reflection can be calculated using the following  
 173 equation:<sup>19</sup>

$$TC_i = \frac{I_i/I_i^0}{1/n \sum_{i=1}^n I_i/I_i^0}$$

176 where  $I_i$  is the experimentally determined intensity  
 177 of the  $i$ th reflection for the textured sample, and  $I_i^0$   
 178 is the calculated or experimentally determined inten-  
 179 sity of the  $i$ th reflection from the randomly oriented  
 180 sample.

181 Figure 3 shows a comparison between the XRD  
 182 patterns taken at room temperature for both pow-  
 183 der and pressed pellet of a typical  $Sr_3GdCo_{3.9}$   
 184  $Ga_{0.1}O_{10.5}$  sample and for a pressed pellet of  
 185  $Sr_3GdCo_4O_{10.5}$ . Although the powders which were  
 186 ground from bulk samples have some degree of  
 187 crystallinity, the intensities of the XRD peaks of the  
 188  $Sr_3GdCo_{3.9}Ga_{0.1}O_{10.5}$  sample are much stronger for  
 189 the pressed surface than for the powders, leading to  
 190 a textured coefficient of  $TC_{33.4^\circ} = 1.92$ . These results



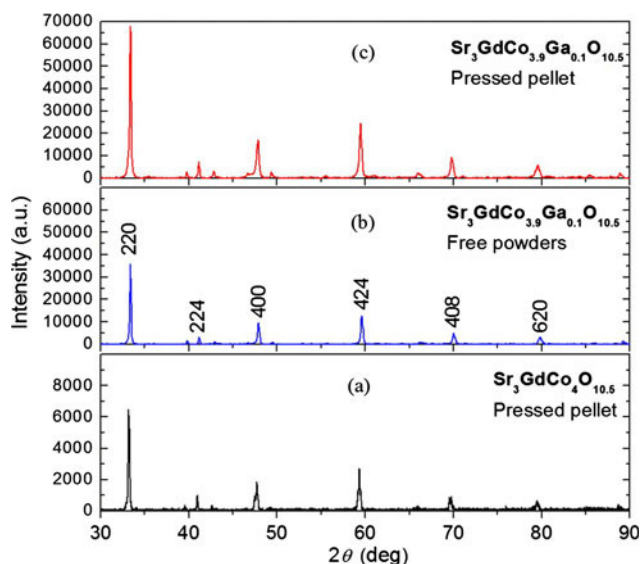


Fig. 3. X-ray diffraction patterns at room temperature for powders and pressed pellets of  $\text{Ca}_3\text{Co}_{4-x}\text{Ga}_x\text{O}_{10.5}$  samples with  $x = 0$  and  $0.1$ .

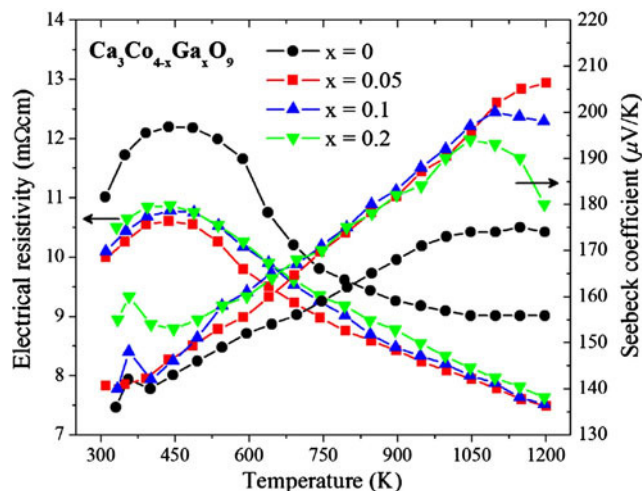


Fig. 5. Temperature dependence of the electrical resistivity and thermoelectric power of  $\text{Ca}_3\text{Co}_{4-x}\text{Ga}_x\text{O}_{9+\delta}$  samples with  $x = 0, 0.05, 0.1, \text{ and } 0.2$ .

Author Proof

191 are consistent with the microstructure observations  
 192 above.  
 193 Figure 4a–d displays SEM images taken from  
 194 fractured cross-sections of the misfit-layered  $\text{Ca}_3\text{Co}_{4-x}\text{Ga}_x\text{O}_9$   
 195 system with  $x = 0, 0.05, 0.1, \text{ and } 0.2$ ,  
 196 respectively. The fractured cross-sections were  
 197 taken roughly perpendicular to the pressure direction  
 198 applied during hot-pressing. A lamella-like struc-  
 199 ture can be observed in all nondoped and Ga-doped

200 samples, but the grain alignment is more pro-  
 201 nounced and better oriented for the Ga-doped ones.  
 202 SEM images again confirm that all the samples with  
 203 Ga substitution are highly textured and highly  
 204 dense, with large crystallographic anisotropy.  
 205 Figure 5 shows the temperature dependence of  
 206 the electrical resistivity and the thermoelectric  
 207 power for  $\text{Ca}_3\text{Co}_{4-x}\text{Ga}_x\text{O}_9$  samples with  $x = 0, 0.05,$   
 208  $0.1, \text{ and } 0.2$ . It can be seen from Fig. 5 that the  $\rho$ - $T$   
 209 curve shows metal-like behavior ( $d\rho/dT < 0$ ) below  
 210 450 K but nonmetallic behavior ( $d\rho/dT > 0$ ) above

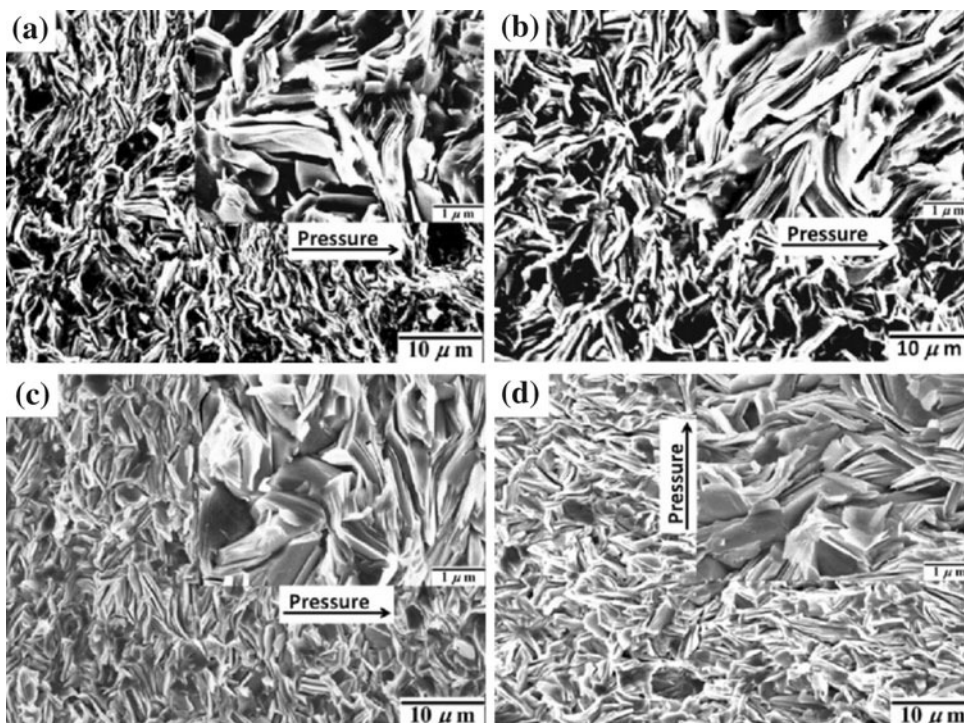


Fig. 4. SEM images of the fractured surfaces roughly perpendicular to the pressure direction of  $\text{Ca}_3\text{Co}_{4-x}\text{Ga}_x\text{O}_{10.5}$  samples: (a)  $x = 0$ , (b)  $x = 0.05$ , (c)  $x = 0.1$ , and (d)  $x = 0.2$ .

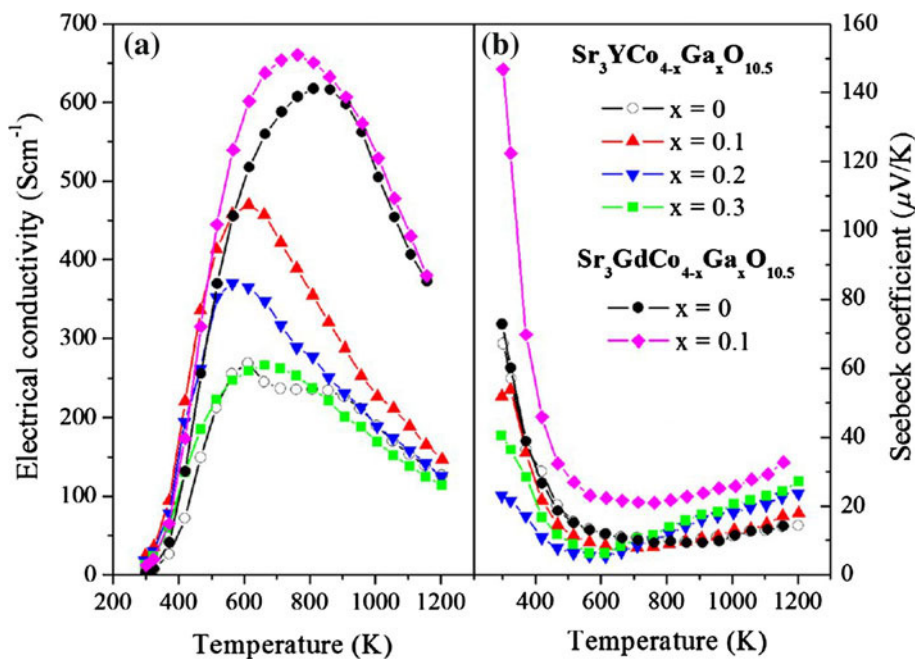


Fig. 6. Temperature dependence of (a) the electrical conductivity, and (b) the thermoelectric power of  $\text{Sr}_3\text{RECo}_{4-x}\text{Ga}_x\text{O}_{10.5}$  for  $0 \leq x \leq 0.3$  with RE = Y and Gd.

450 K, indicating a metal to insulator (M–I) transition.<sup>13,16</sup> Ga substitution for Co causes a decrease of the electrical resistivity in the whole investigated temperature range. Among the Ga-doped samples, the electrical resistivity tends to increase with increasing Ga concentration for  $x > 0.05$ . The Seebeck coefficient of all the samples shows positive values over the measured temperature range, indicating a hole conduction mechanism in these compounds. It is also clear that substitution of Ga for Co results in an increase in the thermoelectric power, and the effect is more significant in the high temperature region ( $T > 600$  K). However,  $S$  decreases with increasing Ga concentration for  $x > 0.05$  in the temperature region  $T > 1050$  K.

Temperature dependence of the electrical conductivity and the Seebeck coefficient of nondoped and Ga-doped  $\text{Sr}_3\text{RECo}_{4-x}\text{Ga}_x\text{O}_{10.5}$  with RE = Y and Gd are shown in Fig. 6a, b, respectively. In general,  $\sigma$ – $T$  curves of the samples increase with increasing temperature, and they decrease rapidly after reaching a maximum at around  $T_{\text{cusp}} = 650 \pm 5$  K and  $810 \pm 5$  K for the samples with RE = Y and Gd, respectively. As is also clearly seen from Fig. 6a, the  $\sigma$  values of the Ga-doped samples are higher than the nondoped one, particularly for the  $x = 0.1$  samples, and the  $T_{\text{cusp}}$  tends to shift to lower temperature. This would be related to the influence of the Ga doping at the Co-site. Among the Ga-doped samples,  $\sigma$  tends to decrease with increasing Ga concentration for  $x > 0.1$ . A possible reason may be due to the fact that the samples with higher Ga content (e.g., for  $x = 0.2$  and  $0.3$ ) contain a secondary phase. In contrast to the electrical conductivity,

the Seebeck coefficient, which also shows  $p$ -type conduction, dramatically decreases with increasing temperature, and it takes a concave shape at temperature that corresponding to the  $T_{\text{cusp}}$  of the  $\sigma$ – $T$  curves. It then increases gradually with further increase of the temperature. The Seebeck coefficient shows a larger value at higher concentration of Ga substitution for Co in the temperature range of  $T > 700$  K. The  $\sigma$  and  $S$  values of all the nondoped and Ga-doped samples from 300 K and 1200 K are listed in Table I, showing that substitution of Ga for Co for  $x \leq 0.1$  results in an increase of both the electrical conductivity and the Seebeck coefficient of the samples at high temperatures. In general, the increase in the electrical conductivity due to the increase of the carrier concentration will also result in a decrease of the thermoelectric power. The simultaneous increase of the electrical conductivity and the thermoelectric power for the Ga-doped samples suggests that such a phenomenon cannot be explained by the above-mentioned general relationship between  $S$  and  $\sigma$ . However, the energy-correlated carrier mobility  $\mu(E)$  may play a crucial role in determining  $S$ . According to Ref. 20, the Seebeck coefficient can be expressed by the following formula:

$$S(T) = \frac{c_e}{n} + \frac{\pi^2 k_B^2 T}{3e} \left[ \frac{\partial \ln \mu(E)}{\partial E} \right]_{E=E_F}, \quad (1)$$

where  $c_e = (\pi^2 k_B^2 T / 3e) N(E)$ , and  $n$ ,  $c_e$ ,  $k_B$ , and  $N(E)$  are the carrier concentration, specific heat, Boltzmann constant, and density of states, respectively. Although the first term  $c_e/n$  of Eq. 1 is inversely



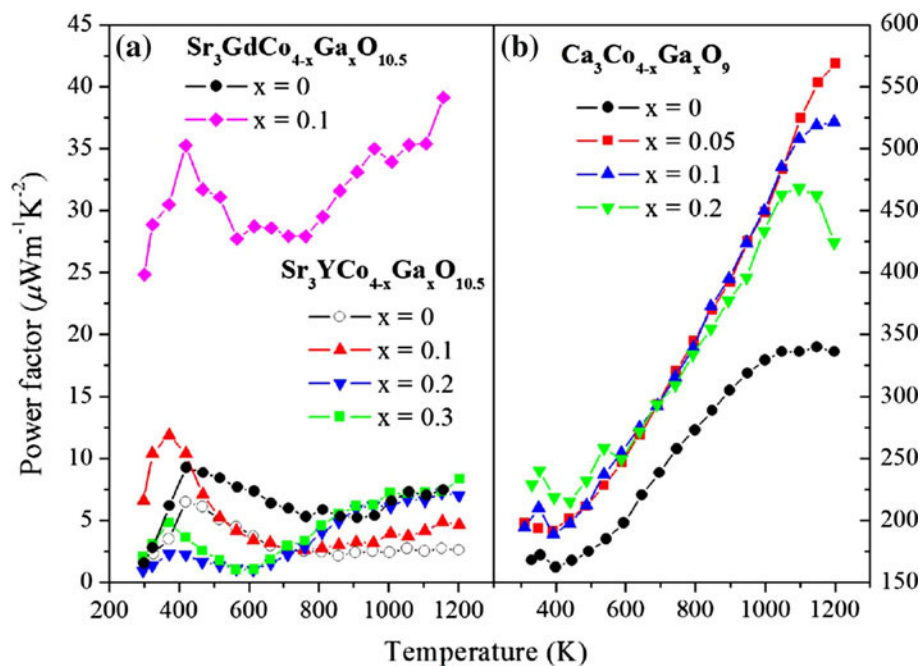


Fig. 7. Temperature dependence of the power factor for: (a)  $\text{Sr}_3\text{RECo}_{4-x}\text{Ga}_x\text{O}_{10.5}$  with  $0 \leq x \leq 0.3$  with RE = Y and Gd, and (b)  $\text{Ca}_3\text{Co}_{4-x}\text{Ga}_x\text{O}_9$  with  $x = 0, 0.05, 0.1,$  and  $0.2$ .

276 proportional to the carrier concentration, the increase of thermoelectric power at high temperature for the Ga-doped samples suggests that the second term may play a dominant role in determining  $S$  for these materials at high temperatures. We could assume that Ga doping for Co occurs at the Co-site having mixed valence of  $\text{Co}^{3+}/\text{Co}^{4+}$ , in which transport properties are dominated by holes. This causes a change in  $\mu(E)$ , and this change affects the increase of  $S$ . Unfortunately, we have not yet obtained data for  $\mu(E)$  from Hall measurements at high temperature. However, evidence from Hall measurements for the Ga-doped  $\text{Ca}_3\text{Co}_{4-x}\text{Ga}_x\text{O}_9$  system at room temperature revealed that the carrier concentration  $n$  and  $\mu$  increased from  $1.97 \times 10^{20} \text{ cm}^{-3}$  and  $0.67 \text{ cm}^2/\text{Vs}$  for the nondoped sample to  $2.34 \times 10^{20} \text{ cm}^{-3}$  and  $1.56 \text{ cm}^2/\text{Vs}$  for the Ga-doped sample with  $x = 0.05$ , respectively. Moreover, a possible reason for why Ga substitutes for Co in the aforementioned Co-site may also stem from their different ionic radii. Considering the usual spin states of these cations, the radius of  $\text{Ga}^{3+}$  (0.62 Å) is close to that of  $\text{Co}^{3+}$  (0.545 Å/0.61 Å, low-spin/high-spin states) and  $\text{Co}^{4+}$  (0.53 Å, low-spin state),<sup>21</sup> so  $\text{Co}^{3+}/\text{Co}^{4+}$  ions can be substituted by the Ga ion. The larger ionic radius of  $\text{Ga}^{3+}$  substitution for Co causes distortion of the structure and hence has a notable effect on carrier transport. However, since the ionic radius of  $\text{Ga}^{3+}$  is larger when compared with  $\text{Co}^{3+}/\text{Co}^{4+}$ , substitution of Ga for Co becomes more difficult with increasing Ga content. This may explain why the Ga-doped  $\text{Sr}_3\text{RECo}_{4-x}\text{Ga}_x\text{O}_{10.5}$  system for  $x \geq 0.2$  showed an impurity phase. As for the  $\text{Ca}_3\text{Co}_{4-x}\text{Ga}_x\text{O}_9$  system,  $\sigma$  and  $S$  tended to

276 decrease with higher Ga concentration for  $x > 0.05$ , e.g.,  $x = 0.1$  and  $0.2$ . In this case  $\text{Ga}^{3+}$  might substitute for  $\text{Co}^{4+}$ , causing a decrease in the  $\text{Co}^{4+}/\text{Co}^{3+}$  ratio, leading to the decrease of hole concentration.

277 As a net result of the simultaneous increase of thermoelectric power and electrical conductivity, the power factor is significantly improved by Ga substitution, as shown in Fig. 7a, b for the complex perovskite and layered-cobalt systems, respectively. The power factor is about  $40 \mu\text{W}/\text{mK}^2$  attained for the  $\text{Sr}_3\text{GdCo}_{4-x}\text{Ga}_x\text{O}_{10.5}$  with  $x = 0.1$ , compared with  $8 \mu\text{W}/\text{mK}^2$  for the nondoped sample at 1200 K. Note that, for the  $\text{Ca}_3\text{Co}_{4-x}\text{Ga}_x\text{O}_9$  system, the power factor of the  $x = 0.05$  sample at 1200 K is  $570 \mu\text{W}/\text{mK}^2$ , which is about 1.7 times larger than that of the nondoped sample. As for the compositions with  $x = 0.1$  and  $0.2$ , the power factor seems to reach a maximum value at a temperature of 1100 K, while the maximum power factor of the  $x = 0.05$  sample has not yet been reached within this range of temperatures.

278 To determine the figure of merit for the Ga-doped layered-cobalt system, the thermal conductivity ( $\kappa$ ) of the nondoped and Ga-doped,  $x = 0.05$  samples were measured and are presented in Fig. 8. For both samples,  $\kappa$  decreases with increasing temperature, and the values are somewhat lower for the Ga-doped sample than for the nondoped one, particularly in the high temperature region ( $T > 400 \text{ K}$ ). Thermal conductivity ( $\kappa_{\text{total}}$ ) can be expressed by the sum of a lattice component ( $\kappa_{\text{ph}}$ ) and an electronic component ( $\kappa_e$ ) as  $\kappa_{\text{total}} = \kappa_{\text{ph}} + \kappa_e$ . In this case, the contribution of  $\kappa_e$  to  $\kappa_{\text{total}}$ , estimated from the Wiedemann–Franz relation, is small,

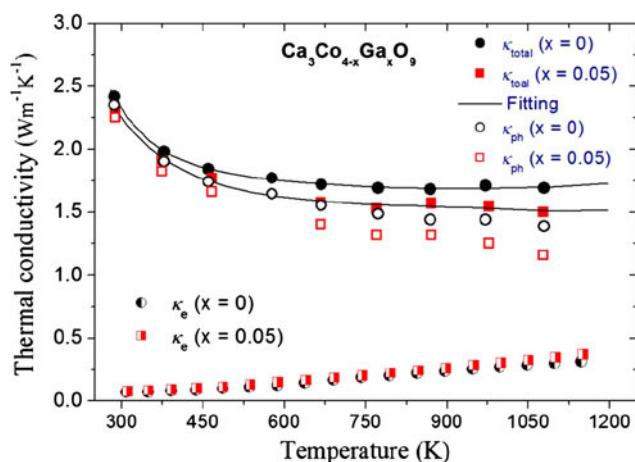


Fig. 8. Electronic and phonon contributions ( $\kappa_e$  and  $\kappa_{ph}$ ) to the thermal conductivity ( $\kappa_{total}$ ) of  $\text{Ca}_3\text{Co}_{4-x}\text{Ga}_x\text{O}_9$  with  $x = 0$  and  $0.05$  as a function of temperature.

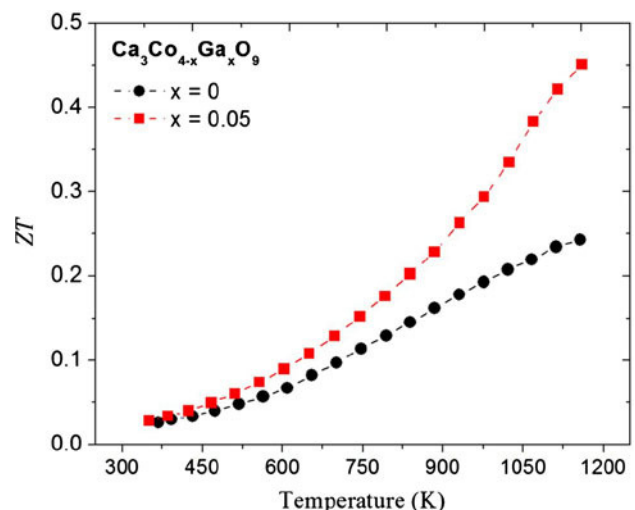


Fig. 9. The dimensionless figure of merit ( $ZT$ ) of  $\text{Ca}_3\text{Co}_{4-x}\text{Ga}_x\text{O}_9$  with  $x = 0$  and  $0.05$  as a function of temperature.

344 indicating the major contribution of the phonon  
 345 term  $\kappa_{ph}$ , as clearly shown in Fig. 8. The decrease in  
 346  $\kappa_{total}$  is therefore attributed to the reduction of lat-  
 347 tice component due to incorporation of heavier  $\text{Ga}^{3+}$   
 348 compared with  $\text{Ca}^{2+}$  ions. Figure 9 presents the  
 349 dimensionless figure of merit,  $ZT$ , versus tempera-  
 350 ture for the  $x = 0$  and  $x = 0.05$  samples, showing  
 351 that  $ZT$  is significantly improved, particularly in the  
 352 high temperature region. The  $ZT$  value of the  
 353  $x = 0.05$  samples could reach 0.45 at about 1200 K.

### 354 CONCLUSIONS

355 We have investigated the effects of Ga substitu-  
 356 tion on the Co-site on the high-temperature ther-  
 357 moelectric (TE) properties and microstructure of a  
 358 series of samples for the complex perovskite  
 359  $\text{Sr}_3\text{RECo}_{4-x}\text{Ga}_x\text{O}_{10.5}$  (RE = Y and Gd) for  $0 \leq x \leq 0.3$

and the misfit-layered  $\text{Ca}_3\text{Co}_{4-x}\text{Ga}_x\text{O}_9$  ( $0 \leq x \leq 0.2$ )  
 systems. Substitution of Ga resulted in simulta-  
 neously increase of the electrical conductivity and  
 the thermoelectric power. This effect is more sig-  
 nificant in the high temperature region. Observa-  
 tion of the microstructure indicated that Ga could  
 act as a sintering aid, which clearly enhanced  
 crystallographic texture, leading to higher density  
 of the samples. The thermoelectric power factor was  
 effectively improved by partial Ga substitution,  
 particularly for the  $\text{Sr}_3\text{GdCo}_{3.9}\text{Ga}_{0.1}\text{O}_{10.5}$  and  $\text{Ca}_3\text{-}$   
 $\text{Co}_{3.95}\text{Ga}_{0.05}\text{O}_9$  samples. A maximum  $ZT$  value of  
 about 0.45 could be obtained for  $\text{Ca}_3\text{Co}_{3.95}\text{Ga}_{0.05}\text{O}_9$   
 at 1200 K, suggesting a promising oxide material  
 for power generation from high-temperature waste  
 heat.

### REFERENCES

1. P.M. Raccach and J.B. Goodenough, *Phys. Rev.* 155, 932 (1967). doi:10.1103/PhysRev.155.932.
2. S. Kimura, Y. Maeda, K. Kashiwagi, H. Yamaguchi, M. Hagiwara, S. Yoshida, I. Terasaki, and K. Kindo, *Phys. Rev. B* 78, 180403 (2008). doi:10.1103/PhysRevB.78.180403.
3. G. Briceno, H. Chang, X. Sun, P.G. Schultz, and X.D. Xiang, *Science* 270, 273 (1995).
4. I. Terasaki, Y. Sasago, and K. Uchinokura, *Phys. Rev. B* 56, R12685 (1997). doi:10.1103/PhysRevB.56.R12685.
5. M. Shikano and R. Funahashi, *Appl. Phys. Lett.* 82, 1851 (2003). doi:10.1143/JJAP.45.4152.
6. T. He, J. Chen, T.G. Calvarese, and M.A. Subramanian, *Solid State Sci.* 8, 467 (2006). doi:10.1016/j.solidstate sciences.2006.01.002.
7. S. Yoshida, W. Kobayashi, T. Nakano, I. Terasaki, K. Matsubayashi, Y. Uwatoko, I. Grigoraviciute, M. Karppinen, and H. Yamauchi, *J. Phys. Soc. Jpn.* 78, 094711 (2009). doi:10.1143/JPSJ.78.094711.
8. J.W. Moon, Y. Masuda, W.S. Seo, and K. Koumoto, *Mater. Lett.* 48, 225 (2001).
9. Y. Wang, Y. Sui, J. Cheng, X. Wang, J. Miao, Z. Liu, Z. Qian, and W. Su, *J. Alloys Compd.* 448, 1 (2008). doi:10.1016/j.jallcom.2006.10.047.
10. F.P. Zhang, Q.M. Lu, and J.X. Zhang, *Phys. B* 404, 2142 (2009). doi:10.1016/j.physb.2009.04.002.
11. M. Prevel, E.S. Reddy, O. Perez, W. Kobayashi, I. Terasaki, C. Goupil, and J.G. Noudem, *Jpn. J. Appl. Phys.* 46, 6533 (2007). doi:10.1143/JJAP.46.6533.
12. H.Q. Liu, X.B. Zhao, T.J. Zhu, Y. Song, and F.P. Wang, *Curr. Appl. Phys.* 9, 409 (2009). doi:10.1016/j.cap.2008.03.010.
13. D. Wang, L. Cheng, Q. Yao, and J. Li, *Solid State Commun.* 129, 615 (2004). doi:10.1016/j.ssc.2003.11.045.
14. Y. Fujine, H. Fujishiro, K. Suzuki, Y. Kashiwada, and M. Ikebe, *J. Magn. Magn. Mater.* 272–276, 104 (2004). doi:10.1016/j.jmmm.2003.11.045.
15. C.J. Liu, L.C. Huang, and J.S. Wang, *Appl. Phys. Lett.* 89, 204102 (2006). doi:10.1063/1.2390666.
16. Y. Wang, Y. Sui, X. Wang, W. Su, and X. Liu, *J. Appl. Phys.* 107, 033708 (2010). doi:10.1063/1.3291125.
17. D. Grebille, S. Lambert, F. Bouree, and V. Petricek, *J. Appl. Crystallogr.* 37, 823 (2004). doi:10.1107/S0021889804018096.
18. C.D. Ling, K. Aivazian, S. Schmid, and P. Jensen, *J. Solid State Chem.* 180, 1446 (2007). doi:10.1016/j.jssc.2007.02.016.
19. M.H. Mueller, W.P. Chernock, and P.A. Beck, *Trans. Metall. Soc. AIME* 212, 39 (1958).
20. G. Xu, R. Funahashi, M. Shikano, Q. Pu, and B. Liu, *Solid State Commun.* 124, 73 (2002). doi:10.1016/S0038-1098(02)00495-7.
21. R.D. Shanon, *Act. Cryst.* A32, 751 (1976). doi:10.1107/S0567739476001551.

